Available online at website: https://journal.bcrec.id/index.php/bcrec

Bulletin of Chemical Reaction Engineering & Catalysis, 21 (4) 2026, 812-824

Original Research Article

Microwave-Assisted Synthesis of Bismuth Silicate (Bi_2SiO_5) from Natural Tunisian Sand for Efficient Solar Photocatalytic Degradation of Rhodamine B

Khouloud Benmarzoug[1,2,*], Chrifa Guerfel[1], Mariem Ahbil[1,2], Noureddine Hamdi[3], Hédi Ben Amor[1]

[1]Laboratory of Research: Processes, Energy, Environment & Electrical Systems PEESE (LR18ES34), National Engineers School, University of Gabes, Street Omar Ibn El Khatab, 6029 Gabes, Tunisia.
[2]Higher institute of Water Sciences and Techniques, ISSTEG, University of Gabes, Zrig 6072, Tunisia.
[3]Laboratory of Composite Materials and Clay Minerals, National Center for Research in Materials Sciences (CNRSM), Soliman 8027, Tunisia.

Received: 23th July 2026; Revised: 7th August 2026; Accepted: 8th August 2026
Available online: 9th August 2026; Published regularly: December 2026

Abstract

The contamination of aquatic environments by synthetic dyes such as Rhodamine B (RhB) represents a growing environmental and public health concern. In this work, a bismuth silicate composite (Bi_2SiO_5) was successfully synthesized via a rapid microwave-assisted co-precipitation route using silica extracted from natural Tunisian sand as a sustainable and low-cost precursor. The material was systematically characterized by XRD, FTIR, UV-Vis DRS, SEM, TEM, and EDX analyses, revealing a highly crystalline orthorhombic structure with an average crystallite size of 57.1 nm (Debye–Scherrer), primary particle dimensions of approximately 43.1 nm, and an optical bandgap of 2.74 eV. Under simulated solar irradiation, Bi_2SiO_5 achieved near-complete decolorization (≈ 99 %) of RhB within 15 min and a significant Chemical Oxygen Demand (COD) removal efficiency of 75 % after 50 min, demonstrating substantial organic scaffold breakdown. Non-linear Kinetic analysis revealed that RhB degradation followed pseudo-first order (PFO) kinetics (k_1 = 0.142 min^{-1}, R^2 = 0.962). Radical Scavenger experiments identified $^{\cdot}OH$ and $^{\cdot}O_2^-$ as the dominant reactive species, with h^+ playing a secondary role, indicating a radical-mediated oxidative degradation mechanism. Bi_2SiO_5 demonstrated good reusability over five consecutive cycles, retaining 95% RhB removal efficiency after the fifth run. These findings establish Bi_2SiO_5 as a promising, eco-friendly photocatalyst derived from abundant natural resources for solar-driven wastewater remediation.

Keywords: Bismuth silicate; Natural sand; Microwave synthesis; Photocatalysis; Rhodamine B; Reactive oxygen species

How to Cite: Benmarzoug, K., Guerfel, C., Ahbil, M., Hamdi, N., Ben Amor, H. (2026). Microwave-Assisted Synthesis of Bismuth Silicate (Bi2SiO5) from Natural Tunisian Sand for Efficient Solar Photocatalytic Degradation of Rhodamine B. *Bulletin of Chemical Reaction Engineering & Catalysis*, 21 (4), 812-824. (DOI: 10.9767/bcrec.20804)

Permalink/DOI: https://doi.org/10.9767/bcrec.20804

1. Introduction

The rapid expansion of global industrial activities, particularly within the textile sector, has led to the widespread discharge of synthetic dyes into aquatic ecosystems, posing severe threats to environmental stability and human health. Among these pollutants, Rhodamine B (RhB), a representative stable cationic triarylmethane dye, is notorious for its high chemical persistence, acute toxicity, and potential carcinogenicity [1,2]. Because conventional wastewater treatment methods fail to effectively eliminate RhB due to its refractory aromatic framework, the development of advanced degradation technologies remains an urgent priority. To address this challenge, semiconductor-based advanced oxidation processes (AOPs), specifically heterogeneous photocatalysis, have emerged as a highly

* Corresponding Authors.
Email: khouloudbenmarzoug12@gmail.com (K. Benmarzoug)

promising strategy for environmental remediation. This technology offers the unique advantage of harnessing solar energy to generate highly reactive oxygen species (ROS), which can non-selectively mineralize organic pollutants into benign end-products, primarily CO_2 and H_2O [3-5]. Among the various photocatalytic materials, bismuth-based semiconductors, notably binary bismuth silicates (e.g., Bi_2SiO_5, $Bi_{12}SiO_{20}$), have attracted intense scientific interest owing to their unique layered structures, adjustable bandgap architectures, and excellent chemical stability [3,6,7]. In particular, the Aurivillius-phase Bi_2SiO_5 is highly regarded for its distinguished electronic properties, which promote superior mobility of photogenerated charge carriers [1,5,7]. To overcome these drawbacks, anchoring or integrating bismuth species onto porous substrate matrices such as silica (SiO_2) has been widely explored. Amorphous silica serves as an ideal support matrix due to its high specific surface area, thermal and chemical robustness, and capability to enhance the overall mechanical strength of the resulting composite [8,9]. While most reported protocols rely on expensive, high-purity commercial precursors (e.g., tetraethyl orthosilicate [TEOS] or sodium silicate), there is an increasing drive toward utilizing natural sand as a low-cost, abundant, and sustainable silica source [10]. Simultaneously, the choice of synthetic methodology plays a decisive role in defining catalytic performance. Microwave (MW)-assisted processing offers substantial advantages over conventional hydrothermal heating, providing rapid, uniform volumetric heating and accelerated reaction kinetics, which yield well-defined nanostructures within significantly shortened synthesis times [5,10], as recently demonstrated across various advanced photocatalytic heterojunctions and engineered oxide systems [11-13].

Despite recent developments in rapid microwave-driven material design [11-13], very few studies have explored the direct valorisation of natural silica sources under microwave irradiation for the fabrication of Bi_2SiO_5. To the best of our knowledge, no previous work has combined natural Tunisian sand-derived silica with a fully open-vessel microwave route for solar photocatalytic dye remediation [4,14]. To bridge this scientific gap, the present study establishes an eco-friendly and rapid microwave route (15 min) utilizing silica extracted from local natural sand (Douiret, Tataouine, Tunisia).

The key novelties of this work include: (i) demonstrating that natural sand-derived silica can successfully replace synthetic precursors to yield photoactive orthorhombic Bi_2SiO_5; (ii) showing that microwave irradiation accelerates phase crystallization compared to traditional thermal aging; and (iii) directly correlating structural, morphological, optical (E_g = 2.74 eV), and surface functional properties with enhanced solar-driven ROS ($^{\bullet}OH$ and $^{\bullet}O_2^-$) generation for dye degradation and chemical oxygen demand (COD) abatement.

Herein, we report the rapid, microwave-assisted synthesis of a Bi_2SiO_5 photocatalyst utilizing naturally derived silica extracted from local Tunisian sand as an eco-friendly precursor, thereby establishing a sustainable and cost-effective pathway for catalyst fabrication. The structural, optical, vibrational, and morphological properties of the synthesized material were systematically investigated using XRD, FTIR, UV-Vis DRS, and SEM/TEM-EDX techniques. Furthermore, the photocatalytic activity of Bi_2SiO_5 was rigorously evaluated for the decolorization and degradation of RhB under both dark (adsorption equilibrium) and natural solar-light irradiation. Finally, scavenger experiments and reusability tests across multiple consecutive cycles were conducted to establish the dominant reactive species and the long-term operational stability of the catalyst for industrial wastewater remediation.

2. Materials and Method

2.1. Materials

The silica used in this study was extracted from natural sand collected from Douiret (Tataouine, Tunisia) via an alkaline fusion process assisted by microwave irradiation. Bismuth nitrate pentahydrate ($Bi(NO_3)_3.5H_2O$, Sigma-Aldrich, 98%), nitric acid (HNO_3, Sigma-Aldrich, 65%), hydrochloric acid (HCl, Merck, 37%), sodium hydroxide (NaOH, Sisco, 97%) and silver nitrate ($AgNO_3$, Sigma-Aldrich, 99%) were of analytical grade and used as received without further purification. Rhodamine B (RhB, Sigma-Aldrich, 95%) was used as the model organic pollutant for photocatalytic degradation experiments. Isopropanol (IPA, Sigma-Aldrich, ≥ 99.5%), *p*-benzoquinone (BZQ, Sigma-Aldrich, ≥ 98%), and disodium ethylenediaminetetraacetate (EDTA-2Na, Sigma-Aldrich, ≥ 99%) were employed as radical scavenger agents, were prepared as 1.0 mM stock solutions.

For Chemical Oxygen Demand (COD) measurements, potassium bichromate ($K_2Cr_2O_7$, Sigma-Aldrich, ≥ 99%), silver sulfate (Ag_2SO_4, Sigma-Aldrich, ≥ 99.5%) dissolved in concentrated sulfuric acid (H_2SO_4, Merck, 98%) and mercury(II) sulfate masking agent ($HgSO_4$, Sigma-Aldrich, ≥ 98.0%) were utilized for sample digestion according to standard procedures, followed by spectrophotometric quantification of COD content via absorbance measurement at 420 nm. Distilled water was used throughout all experimental procedures.

2.2. Synthesis of Bi_2SiO_5

Bi_2SiO_5 was synthesized via a rapid microwave-assisted co-precipitation route (Figure 1), developed following established microwave-assisted co-precipitation approaches reported in the literature [6]. The primary innovation lies in the use of naturally derived silica nanoparticles (SiNPs) extracted from natural sand as a low-cost, eco-friendly precursor instead of industrial sodium silicate [10]. Furthermore, the traditional time-consuming hydrothermal treatment in an autoclave was replaced by direct microwave-induced crystallization at ambient pressure, and conventional furnace calcination was substituted with a high-power microwave thermal treatment, drastically reducing the total fabrication time from hours to minutes [10].

In a typical procedure, 4.85 g of $Bi(NO_3)_3 \cdot 5H_2O$ were dissolved in 1 mL of concentrated HNO_3 (65%) and then diluted with distilled water to a final volume of 50 mL under gentle stirring overnight (250 rpm), ensuring the formation of a homogeneous precursor solution. Subsequently, 20 mL of this bismuth solution were added to a three-neck flask containing 0.25 g of the sand-derived silica support, maintaining a constant molar ratio of R(Bi/Si) = 1. The suspension pH was adjusted to 10.4 using a 2 M NaOH solution (measured with a Bicasa Digital Thermo pH Meter mod. B.E.105), followed by 20 min of vigorous stirring (250 rpm) at room temperature (25 ± 2°C) to facilitate homogeneous precipitation of bismuth species onto the silica surface [15]. The resulting mixture was then subjected to microwave irradiation at 160 W for only 5 min in an open-vessel configuration using a modified microwave system (Samsung ME711K, operating at a frequency of 2.45 GHz) avoiding the need for high-pressure autoclave conditions [16].

After cooling, the precipitate was recovered by centrifugation (Gyrozen 416 Centrifuge) at 2500 rpm for 10 min and washed repeatedly with distilled water. Washing was continued until the filtrate reached a neutral pH (≈ 7.0) and returned to the baseline electrical conductivity of distilled water (measured with a Hach Conductivity/TDS Meter). Finally, the purified solid underwent rapid microwave calcination at 750 W for 10 min, in the same Samsung ME711K microwave system (2.45 GHz), yielding Bi_2SiO_5 as a yellow powder. The final product was stored in an airtight container to maintain its structural integrity and surface properties prior to characterization [10].

2.3. Characterizations

The physicochemical properties of the synthesized material were investigated using several complementary analytical techniques. The XRD patterns were acquired on a Bruker D8 Advance diffractometer equipped with a Cu-Kα1 source and a Lynxeye XE-T detector, recording the 2θ range from 0-70° at scan step of 1.8 min^{-1}. The Debye-Scherrer equation was used to calculate the average crystallite size [17]:

$$D = \frac{K\lambda}{\beta \cos\theta} \quad (1)$$

where D is the crystallite size (nm), K is the shape factor, λ is the X-ray wavelength, β is the full width at half maximum (FWHM, in radians), and θ is the Bragg diffraction angle (in radians).

The relative weight percentages of the predominant orthorhombic Bi_2SiO_5 phase and the minor Bi_2O_3 phase were calculated by semi-quantitative XRD intensity integration using the following equation:

$$W_{Bi_2SiO_5}(\%) = \left(\frac{I_{Bi_2SiO_5}}{I_{Bi_2SiO_5} + I_{Bi_2O_3}}\right) \times 100 \quad (2)$$

where $I_{Bi2SiO5}$ represents the integrated intensity of the principal reflection and I_{Bi2O3} corresponds to the secondary phase reflection.

Fourier-transform infrared spectroscopy (FTIR), (JASCO FT/IR-6X) was used to identify surface functional groups and chemical bonds in the sample over a wavenumber range of 4000-400 cm^{-1} with a spectral resolution of 4 cm^{-1}. UV-Vis diffuse reflectance spectra (DRS) were acquired using a Cary 100 Scan spectrophotometer

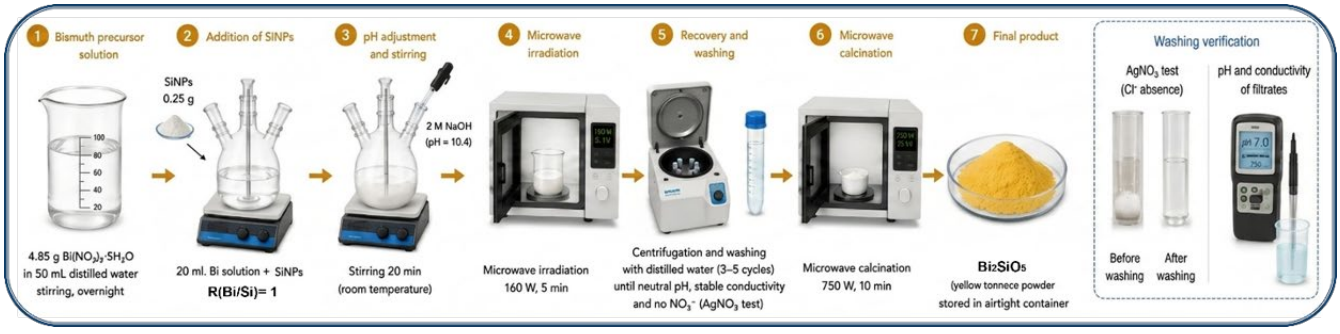

Figure 1. Schematic mechanism of the ultra-fast microwave-assisted solid-state synthesis of monocrystalline Bi_2SiO_5 using natural sand-derived SiNPs.

equipped with an integrating sphere accessory over the wavelength range of 200-800 nm, using $BaSO_4$ as the baseline reference. The optical bandgap energy (E_g) was determined from the DRS spectrum using Tauc plot extrapolation assuming a direct electronic transition. Surface morphology, microstructural features, and elemental composition were examined using scanning electron microscopy (SEM) coupled with energy-dispersive X-ray spectroscopy (EDS), (JEOL JSM-6700F) allowing determination of both the surface texture and elemental composition of the material. In addition, transmission electron microscopy (TEM) micrographs of the sample were acquired on a JEOL JEM1400 operating at 120 kV, producing high-resolution images that enabled clear differentiation between single-crystal, polycrystalline, and amorphous structures. All characterization analyses were carried out at the research facilities of the University of Vigo, Spain.

2.4. Evaluation of Photocatalytic Performance and COD Mineralization

The photocatalytic performance of the synthesized material was evaluated through the degradation of RhB under simulated solar irradiation using a G2V Pico solar simulator (861 $W.m^{-2}$, corresponding to midday solar intensity in Tunisia). The experimental setup comprised a double-walled glass beaker (7 cm height) placed on a magnetic stirrer vertically beneath the lamp, with a continuous water circulation system to maintain a constant temperature (25 ± 2 °C). In a typical run, the photocatalyst was dispersed in a 1×10^{-5} M RhB solution (50 mL) with a 20 mg catalyst dosage at pH of 3. Prior to illumination, the suspension was magnetically stirred in the dark for 60 min to establish adsorption-desorption equilibrium. The mixture was then exposed to simulated solar light for 15 min. Aliquots were sampled at regular intervals time, centrifuged at 2000 rpm and the residual dye concentration profile was monitored via a Jasco V-770 UV-Vis spectrophotometer at λ_{max} = 554 nm. The photocatalytic degradation efficiency (DE%) was calculated using the following equation:

$$DE\ (\%) = \left(\frac{C_0 - C_t}{C_0}\right) \times 100 \quad (3)$$

where C_0 represents the initial concentration of the pollutant after the dark adsorption period, and C_t is the residual concentration at a given irradiation time t.

Control experiments without the catalyst confirmed that direct photolysis of RhB was negligible. Additionally, photocatalyst reusability was evaluated through successive recycling runs, each maintaining the sequence of 60 min of dark adsorption followed by the 15 min irradiation period. To assess the extent of organic dye mineralization, COD was determined according to the standard closed reflux colorimetric method. Samples were collected at designated irradiation intervals time (t = 0, 5, 10, 20, and 50 min) and centrifuged. Digestion was carried out in an acidic medium using potassium dichromate ($K_2Cr_2O_7$), silver sulfate catalyst (Ag_2SO_4), and mercury(II) sulfate masking agent ($HgSO_4$) in a thermo-reactor at 150 °C for 2 h. After cooling to room temperature, the COD content was quantified spectrophotometrically by measuring absorbance at 420 nm. The COD removal efficiency (%) was calculated using Equation (4):

$$COD\ removal\ efficiency\ (\%) = \left(\frac{COD_0 - COD_t}{COD_0}\right) \times 100\% \quad (4)$$

where COD_0 is the initial COD value, and COD_t is the residual COD value at a given irradiation time t. All photocatalytic degradation and COD experiments were performed in triplicate (n = 3), and reported values represent mean values with a relative experimental error not exceeding 4% across replicates.

2.5. Kinetic studies and Error Analysis

To investigate the reaction rates and mechanisms of RhB photodegradation, the experimental data were fitted using non-linear pseudo-first-order (PFO) and pseudo-second-order (PSO) kinetic models. The non-linear forms of these models are expressed by Equations (5) and (6), respectively [18,19]:

$$C_t = C_0 . e^{-k_1 . t} \quad (5)$$

$$C_t = \frac{C_0}{1 + C_0 . k_2 . t} \quad (6)$$

where k_1 (min^{-1}) and k_2 ($L.mg^{-1}.min^{-1}$) represent the apparent non-linear rate constants for the PFO and PSO models, respectively, and t (min) is the irradiation time. The kinetic parameters were determined via non-linear regression analysis to preserve the original error structure of the experimental data.

The suitability and accuracy of the kinetic models were evaluated using the coefficient of determination (R^2), the sum of squared errors (SSE), and the Chi-square (χ^2) error function [18]. These parameters were calculated according to the following equations:

$$R^2 = 1 - \frac{\sum_{i=1}^{n} (C_{exp,i} - C_{cal,i})^2}{\sum_{i=1}^{n} (C_{exp,i} - C_{mean,i})^2} \quad (7)$$

$$SSE = \sum_{i=1}^{n} \left(C_{exp,i} - C_{cal,i}\right)^2 \quad (8)$$

$$\chi^2 = \sum_{i=1}^{n} \frac{(C_{exp,i} - C_{cal,i})^2}{C_{cal,i}} \quad (9)$$

where $C_{exp,i}$ is the experimental concentration measured at time i, $C_{cal,i}$ is the corresponding concentration calculated from the kinetic model, and $C_{mean,i}$ is the average value of the experimental data. Higher R^2 values (approaching 1.0) coupled with minimized, lower SSE and χ^2 values indicate the highest statistical accuracy and determine the best-fit kinetic model for the pollutant degradation process.

2.6. Reusability and Stability Tests

To assess the long-term stability and recyclability of the Bi_2SiO_5 photocatalyst, five consecutive degradation cycles were carried out under identical simulated solar irradiation conditions for RhB. After each run, the catalyst was recovered by centrifugation, washed sequentially with distilled water and absolute ethanol to eliminate residual adsorbed intermediates, and dried overnight at 60 °C prior to the next cycle. For each run, a fresh RhB solution was prepared at the same initial concentration, and the catalyst dosage was kept constant throughout (20 mg).

3. Results and Discussion

3.1. Structural Characterizations

The crystalline structure and phase characteristics of the synthesized materials were investigated using X-ray diffraction (XRD), as shown in Figure 2a. The XRD pattern of the SiNPs precursor (red curve) exhibits a dual nature, characterized as an amorphous-crystalline state [10]. It shows sharp, well-defined reflections (notably an intense peak near 27°) superimposed on a broad diffuse "hump" between 20° and 30°, indicating that the silica extracted from natural sand retains its crystalline quartz heritage while possessing a disordered nanoparticles framework [10]. Following bismuth incorporation via microwave treatment, the Bi_2SiO_5 pattern (green curve) displays a distinct set of additional sharp, intense reflections concentrated in the 2θ range of 20-35°. These new peaks are accurately indexed to the pure orthorhombic phase of (JCPDS No. 36-0287), confirming that the microwave method effectively facilitates rapid nucleation and growth of crystalline bismuth silicate domains on the silica support [5,14,20]. A minor set of additional low-intensity reflections was also

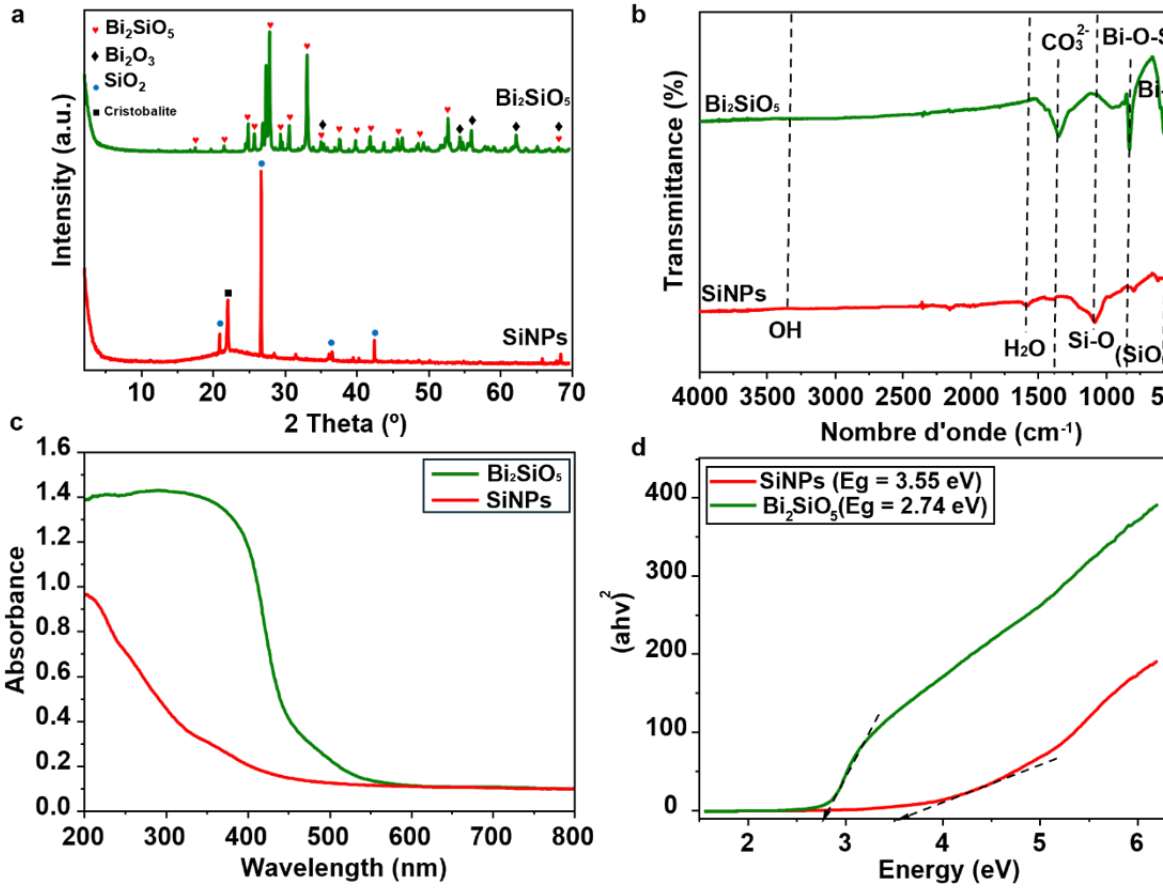

Figure 2. Structural and optical characterization of the synthesized Bi_2SiO_5 and SiNPs samples: (a) XRD patterns, (b) FTIR spectra, (c) UV-Vis diffuse reflectance spectra, and (d) Tauc plots for bandgap (E_g) estimation.

detected and attributed to a secondary Bi_2O_3 phase, consistent with partial, localized excess bismuth nucleation during the rapid microwave-induced crystallization [14].

The mean crystallite size (D) was evaluated using the Debye-Scherrer relationship (Equation 1). Applying this equation to the primary Bi_2SiO_5 reflections at 2θ = 27.83° (FWHM = 0.12°) and 2θ = 33.05° (FWHM = 0.18°) yielded computed crystallite sizes of 68.2 nm and 46.0 nm, respectively, resulting in an average crystallite size of 57.1 nm. This value is in close agreement and of the same order of magnitude as the average primary particle diameter observed by TEM (43.1 nm, Section 3.2), confirming that rapid microwave-assisted synthesis yields highly crystalline nanocomposites with consistent domain and particle dimensions. This nanoscale dimension supports a high active surface area and shortens charge carrier transport distances to the surface, directly benefiting solar light photo-reactivity.

Furthermore, the relative phase distribution was quantified using the semi-quantitative peak area integration method [21] (Equation 2) based on the characteristic reflections at 2θ = 27.83° ($I_{Bi2SiO5}$= 3733 a.u.) and 2θ = 55.3° (I_{Bi2O3}= 240 a.u.). The integrated intensity ratio demonstrates that orthorhombic Bi_2SiO_5 constitutes the predominant active phase (93.03 wt%), accompanied by a minor trace amount of Bi_2O_3 (6.97 wt%). While this semi-quantitative estimation provides a clear indication of high phase purity, full-profile Rietveld refinement is acknowledged as an essential tool for future investigations to achieve higher structural precision and verify absolute phase fractions.

The surface functional groups and chemical bonding were evaluated using FTIR spectroscopy (Figure 2b). Both samples display the characteristic signatures of the silica framework (Si-O-Si) in the 4000-500 cm^{-1} region [20,22,23]. However, the spectrum shows more pronounced features below 600 cm^{-1} and a characteristic band around 830-865 cm^{-1}, which is attributed to the stretching vibrations of Bi-O-Si linkages [1,15]. The emergence of these bands proves that bismuth species are chemically anchored to the silica matrix rather than being a simple physical mixture, a result of the efficient energy transfer during microwave synthesis.

The optical properties were investigated using UV-Vis Diffuse Reflectance Spectroscopy (DRS) (Figure 2c). While pure silica (SiNPs) shows an absorption edge confined to the UV region (below 300 nm), the Bi_2SiO_5 composite exhibits a significant redshift, extending its light-harvesting capability into the visible region up to approximately 400-450 nm [6,8].

To determine the optical bandgap (E_g), Tauc plots were generated assuming a direct electronic transition (Figure 2d) [1,8]. Linear extrapolation of the absorption edges yields an E_g value of 3.55 eV for the SiNPs precursor, which reflects the wide-bandgap, insulating nature of the pure silica matrix. In contrast, the microwave-synthesized Bi_2SiO_5 sample displays a significantly narrower bandgap energy of 2.74 eV. While higher bandgap values, typically ranging from 3.30 eV to 3.89 eV, are frequently reported in the literature for wide-gap bismuth silicate depending on the silica origin, the initial bismuth-to-silica (Bi/Si) precursor ratio, and the specific synthesis conditions [4,5,15]. The E_g value of 2.74 eV obtained in this work is in excellent agreement with recent studies reporting optical thresholds between 2.68 eV and 2.75 eV for highly crystalline, pure-phase orthorhombic Bi_2SiO_5 [7]. This significant bandgap narrowing confirms the successful incorporation of bismuth into the silica network, effectively extending the light-harvesting capability of the material into the visible light region (450 nm).

3.2. Morphological Characterization

The evolution of surface morphology and microstructure was evaluated using TEM and SEM-EDX. TEM images of the unmodified silica (SiNPs) reveal irregular, agglomerated clusters without distinct particle boundaries (Figure 3a, b) [9]. In contrast, after the microwave-assisted incorporation of bismuth, the Bi_2SiO_5 material presents a markedly different morphology consisting of discrete, well-defined spherical and ovoid nanoparticles with a measured average diameter of approximately 43.1 nm (Figure 3c) [10]. At higher particle densities, these nanoparticles aggregate into elongated, chain-like arrangements, indicating that the MW method promotes the organized growth of crystalline domains on the porous silica support [20].

SEM imaging confirms a micro-scale morphology characterized by irregular, plate-like and angular fragments, a texture inherited from the natural sand-derived precursor [9]. The elemental composition was validated through Energy Dispersive X-ray (EDX) spectroscopy (Figure 3f), confirming the presence of Bi, Si, and O, along with minor signals from the natural sand matrix [5,7,9,20]. The spectrum shows a prominent bismuth signal (18.6 wt%), and elemental mapping indicates that the bismuth is uniformly distributed across the sample [7]. This homogeneous distribution supports the mechanism of successful chemical anchoring of bismuth ions within the silica framework, which is essential for achieving high photocatalytic performance.

3.3. Photocatalytic Performance, Kinetics and Mineralization Monitoring (COD)

The photocatalytic performance of the as-prepared Bi_2SiO_5 was evaluated through the degradation of RhB under solar irradiation, following a 60-min dark adsorption equilibration phase. As illustrated in Figure 4a, Bi_2SiO_5 achieved substantial adsorptive removal of RhB during the dark stage, with the C_t/C_0 ratio decreasing from 1.0 to approximately 0.32 within 60 min (corresponding to 68% dark adsorption). This high dark adsorption capability is directly justified by the structural and morphological features identified in Sections 3.1 and 3.2. The disordered nanostructured silica framework derived from natural sand, combined with the discrete spherical/ovoid primary nanoparticles observed by TEM (d_{avg} = 43.1 nm) and small crystallite size (D = 57.1 nm), provides an abundant density of active surface sites, short lattice boundaries, and a favorable porous architecture that promotes strong electrostatic interactions with cationic RhB dye molecules.

Upon solar light irradiation, Bi_2SiO_5 exhibited exceptionally rapid degradation kinetics, achieving near-total decolorization (99%) within 15 min. This outstanding photoactivity is intimately linked to the full set of crystalline, optical, and chemical characterization results. As established by XRD, the rapid microwave-assisted crystallization created well-defined orthorhombic Bi_2SiO_5 domains (JCPDS No. 36-0287) intimately anchored on the silica support. High crystallinity minimizes structural defects that typically act as charge recombination centers, thereby facilitating efficient generation, separation, and migration of photogenerated electron-hole (e^-/h^+)

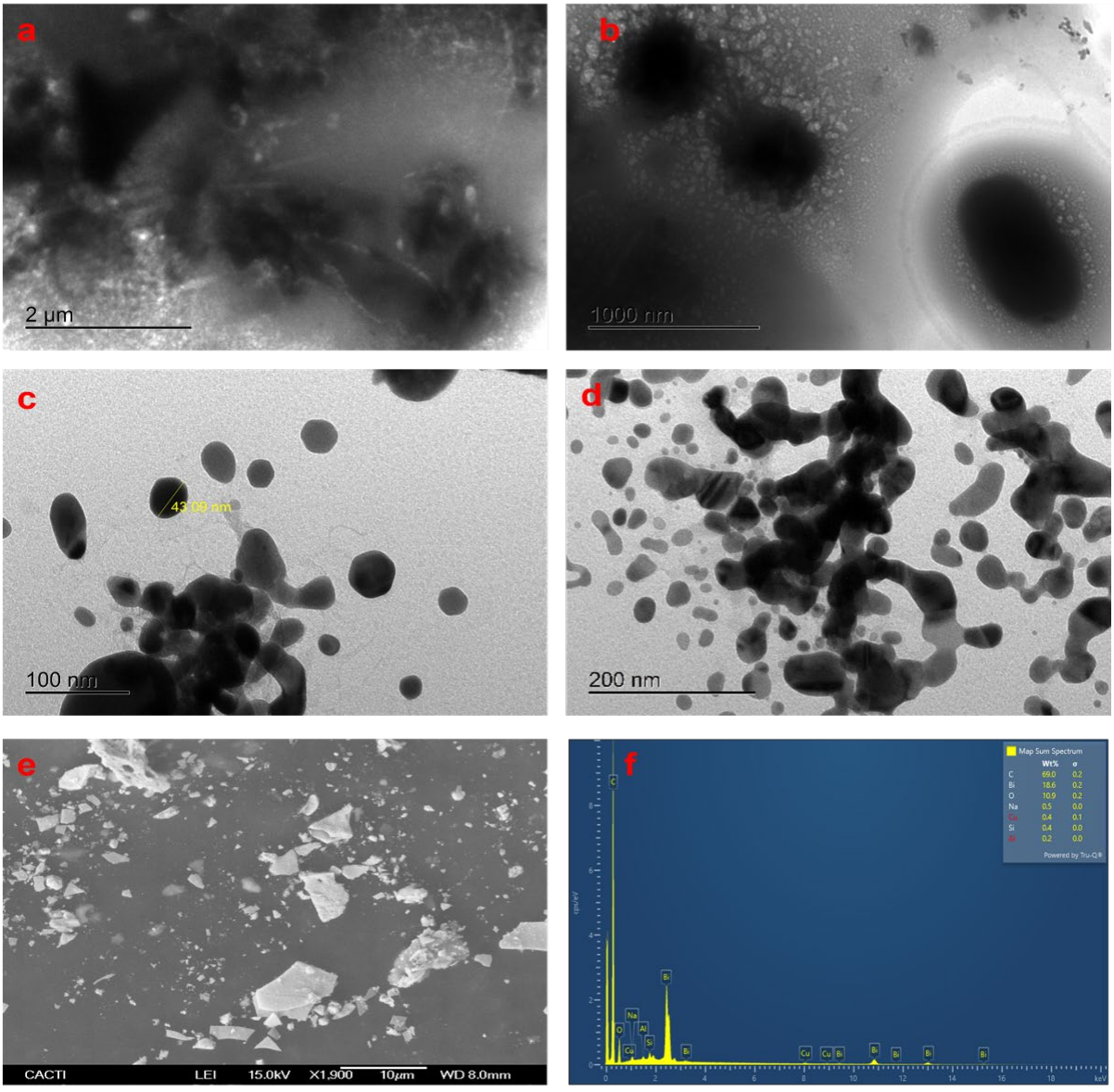

Figure 3. Morphological, microstructural, and elemental analysis of the synthesized Bi_2SiO_5 catalyst: (a, b) TEM micrographs of SiNPs; (c, d) TEM micrographs of Bi_2SiO_5; (e) SEM image of Bi_2SiO_5; (f) EDX spectrum of Bi_2SiO_5.

pairs to the catalyst surface under solar irradiation. Furthermore, this rapid 15 min solar conversion is directly justified by the significant UV-Vis DRS bandgap narrowing from 3.55 eV (pure SiNPs) down to 2.74 eV in Bi_2SiO_5, extending the light absorption threshold well into the visible light region (≈ 450 nm). In addition, the localized secondary Bi_2O_3 phase identified in the XRD patterns can form interfacial heterojunction domains with Bi_2SiO_5, promoting spatial charge carrier separation across the phase boundaries. The chemical anchoring confirmed by FTIR spectroscopy (emergence of Bi-O-Si linkages at 830-865 cm^{-1}) and uniform EDX elemental mapping (18.6 wt% Bi) proves that bismuth species are covalently bound to the matrix rather than physically mixed, creating conductive atomic bridges for rapid charge transport. The close match between the Debye-Scherrer crystallite size (57.1 nm) and primary TEM particle size (43.1 nm) further confirms short carrier diffusion paths (20-40 nm) that prevent volume recombination before charges reach surface dye molecules. In contrast, the control experiment without catalyst (photolysis) showed a negligible decrease in RhB concentration (C_t/C_0 remaining close to 1.0) throughout the entire dark and illuminated periods, confirming that the observed degradation is exclusively attributable to the photocatalytic activity of Bi_2SiO_5 and not to direct photolysis [23].

To investigate the reaction pathways and rate-controlling mechanisms of RhB removal, the experimental degradation profile over Bi_2SiO_5 was fitted using the non-linear forms of the PFO and PSO kinetic models [18,19]. The use of non-linear regression analysis is preferred as it determines kinetic parameters while preserving the original error structure of the experimental data, which can be distorted during linear transformations [18]. As summarized in Table 1 and illustrated in Figure 4b, the PFO model provided a superior fit (R^2 = 0.962) with substantially lower error values (χ^2 = 0.415, SSE = 0.140) compared to the PSO model (R^2 = 0.864, χ^2 = 1.113, SSE = 0.297). This clear preference for the PFO model indicates that the RhB degradation rate over Bi_2SiO_5 is primarily governed by the concentration of dye molecules remaining in the bulk solution, a behavior typical for ionic dyes in dilute systems [19]. The apparent rate constant (k_1 = 0.142 min^{-1}) is consistent with the exceptionally rapid removal observed experimentally, which is ultimately driven by the synergism between the high adsorption capacity (68%) of the silica framework and the rapid charge-transfer kinetics enabled by the narrowed bandgap (2.74 eV), covalent Bi-O-Si linkages, and crystalline domain architecture of the Bi_2SiO_5 nanocomposite.

Table 1. Non-linear kinetic parameters for PFO and PSO models applied to the photocatalytic degradation of RhB over Bi_2SiO_5.

Model	k	χ^2	R^2	SSE
PFO	0.142 (min^{-1})	0.415	0.962	0.140
PSO	0.096 ($L.mg^{-1}.min^{-1}$)	1.113	0.864	0.297

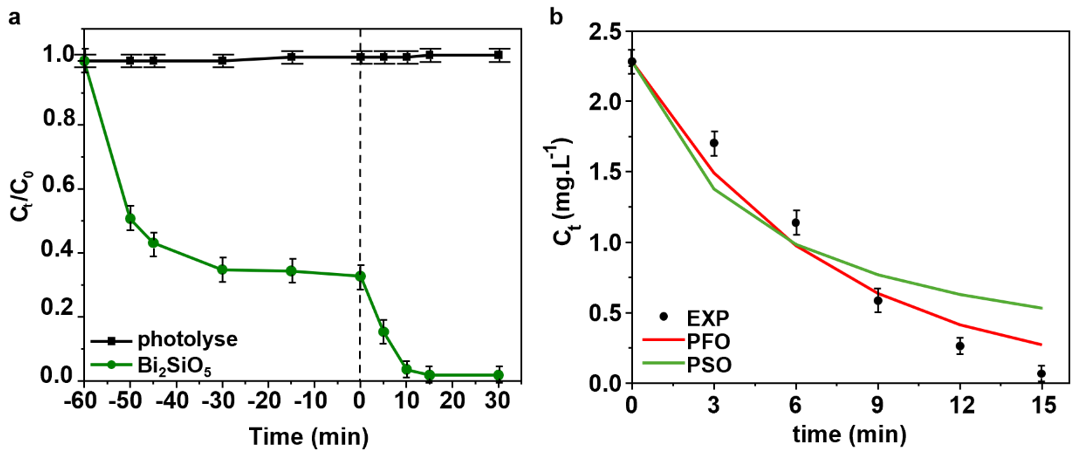

Figure 4. Photocatalytic degradation of RhB over Bi_2SiO_5: (a) dark adsorption/degradation profile with photolysis control; (b) PFO and PSO kinetic fitting.

To verify true organic mineralization rather than simple color bleaching, COD was measured at t = 0, 5, 10, 20, and 50 min. As shown in Figure 5, the initial COD decreased from 11.45 mg O_2/L to 2.90 mg O_2/L after 50 min of solar treatment, achieving a total COD reduction of 75%. This significant drop confirms that solar photocatalysis over Bi_2SiO_5 breaks down the complex aromatic framework of RhB, converting organic intermediates into aliphatic organic acids as well as harmless inorganic end-products (CO_2, H_2O, and mineral ions).

3.4. Reusability and Stability

The long-term stability and reusability of the sand-derived Bi_2SiO_5 composite were evaluated through five consecutive photocatalytic runs for the removal of RhB under simulated solar light, as this is a fundamental criterion for assessing the feasibility of photocatalysts in industrial wastewater remediation [24,2]. Following each cycle, the material was recovered via centrifugation, washed thoroughly with distilled water and ethanol to eliminate adsorbed intermediate fragments, and dried before being reintroduced into a fresh RhB solution [2,25]. As illustrated in Figure 6, Bi_2SiO_5 exhibited excellent structural robustness and performance retention across the five cycles, with the RhB removal efficiency decreasing only slightly from 99% in the first run to 95% by the fifth run. This marginal reduction in photocatalytic activity is consistent with findings for bismuth silicate systems and is primarily attributed to the unavoidable physical loss of catalyst powder during recovery and potential surface fouling caused by the accumulation of persistent degradation intermediates on the active Bi-O-Si linkages [5,9,24]. These results establish Bi_2SiO_5 as a stable, durable, and cost-effective candidate for the continuous remediation of organic dye contaminants under natural sunlight [5,9,24].

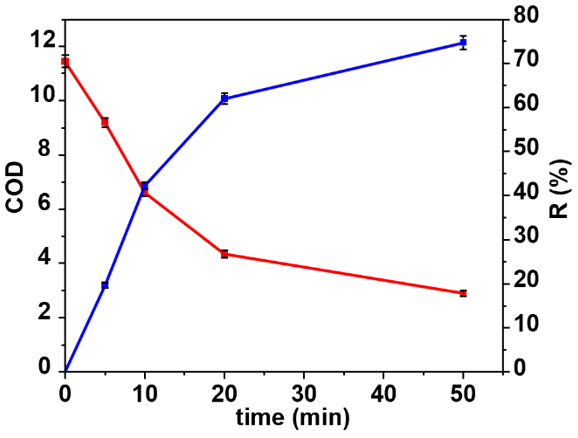

Figure 5. Evolution of COD concentration (red curve) and COD removal efficiency (R %, blue curve) as a function of treatment time. (RhB Initial concentration = 1×10^{-5} M, m (Bi_2SiO_5) = 40 mg, Volume = 100 mL, pH = 3, t = 50 min, and at room temperature).

3.5. Proposed Photocatalytic Mechanism and Identification of Reactive Species

To identify the primary reactive oxygen species (ROS) responsible for the degradation of RhB and to elucidate the underlying photocatalytic mechanism, scavenger trapping experiments were performed over Bi_2SiO_5. In these tests, isopropanol (IPA), p-benzoquinone (BZQ), and disodium ethylenediaminetetraacetate (EDTA-2Na) were employed as selective quenchers for hydroxyl radicals (·OH), superoxide radicals (•O_2^-), and photogenerated holes (h^+), respectively [26,27].

As illustrated in Figure 7, the RhB removal efficiency decreased sharply upon the addition of IPA and BZQ, dropping from approximately 99% (no scavenger) to approximately 14% and 18%, respectively. This dramatic suppression confirms

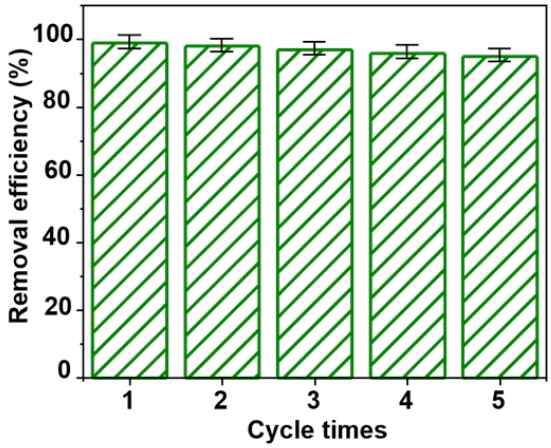

Figure 6. Reusability of Bi_2SiO_5 over five consecutive photocatalytic cycles for RhB degradation.

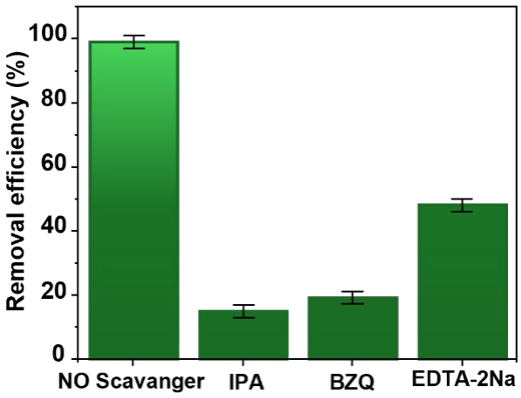

Figure 7. Effect of radical scavengers on the photocatalytic removal efficiency of RhB over Bi_2SiO_5.

that ·OH and $\cdot O_2^-$ are the dominant active species driving the oxidation process in this sand-derived bismuth silicate system [4]. In contrast, the introduction of EDTA-2Na resulted in a more moderate decrease, with removal efficiency falling to approximately 48%, indicating that while photogenerated holes (h^+) contribute to the mechanism, their role is secondary compared to the radical-mediated pathways. These findings are consistent with reports on hierarchical bismuth silicate structures, where $\cdot O_2^-$ and ·OH are identified as the main drivers for the mineralization of ionic dyes [4,5].

The generation of these ROS is governed by the electronic band behavior of the composite (Figure 8). Upon solar light excitation, photogenerated electrons (e^-) in the conduction band (CB) reduce dissolved oxygen molecules to generate $\cdot O_2^-$. Simultaneously, the holes (h^+) remaining in the valence band (VB) can oxidize surface-adsorbed water or hydroxyl groups to yield •OH [5,19]. The significant involvement of both radicals underscores the efficient spatial separation and transfer of photogenerated charge carriers, a process facilitated by the Bi-O-Si linkages acting as bridges within the silica framework [1]. While the proposed degradation pathway is adequately supported by radical trapping measurements, future investigations utilizing photoluminescence (PL), transient photocurrent response, electrochemical impedance spectroscopy (EIS), and electron spin resonance (ESR) will provide direct spectroscopic confirmation of charge carrier dynamics and radical generation.

3.6 Comparison with Literatures

The photocatalytic performance of the sand-derived Bi_2SiO_5 composite was benchmarked against various bismuth-based photocatalysts reported in the literature to highlight the efficiency and sustainability of the current approach (Table 2). A primary highlight of this study is the synthesis efficiency; while conventional hydrothermal and solvothermal methods often require between 12 and 24 hours in high-pressure autoclaves to achieve crystalline bismuth silicate phases [4,14,25] and up to 24 h for binary TiO_2/Bi_2SiO_5 heterojunctions synthesized via hydrothermal routes [7],our open-vessel microwave-assisted co-precipitation route yielded a high-performance composite in only 5-10 min.

To evaluate the degradation efficiency objectively, the performance reported in Table 2 must be evaluated alongside the varying operational parameters, including initial RhB concentration (C_0), catalyst loading, light source spectrum, and synthesis energy inputs, rather than concluding superiority based solely on

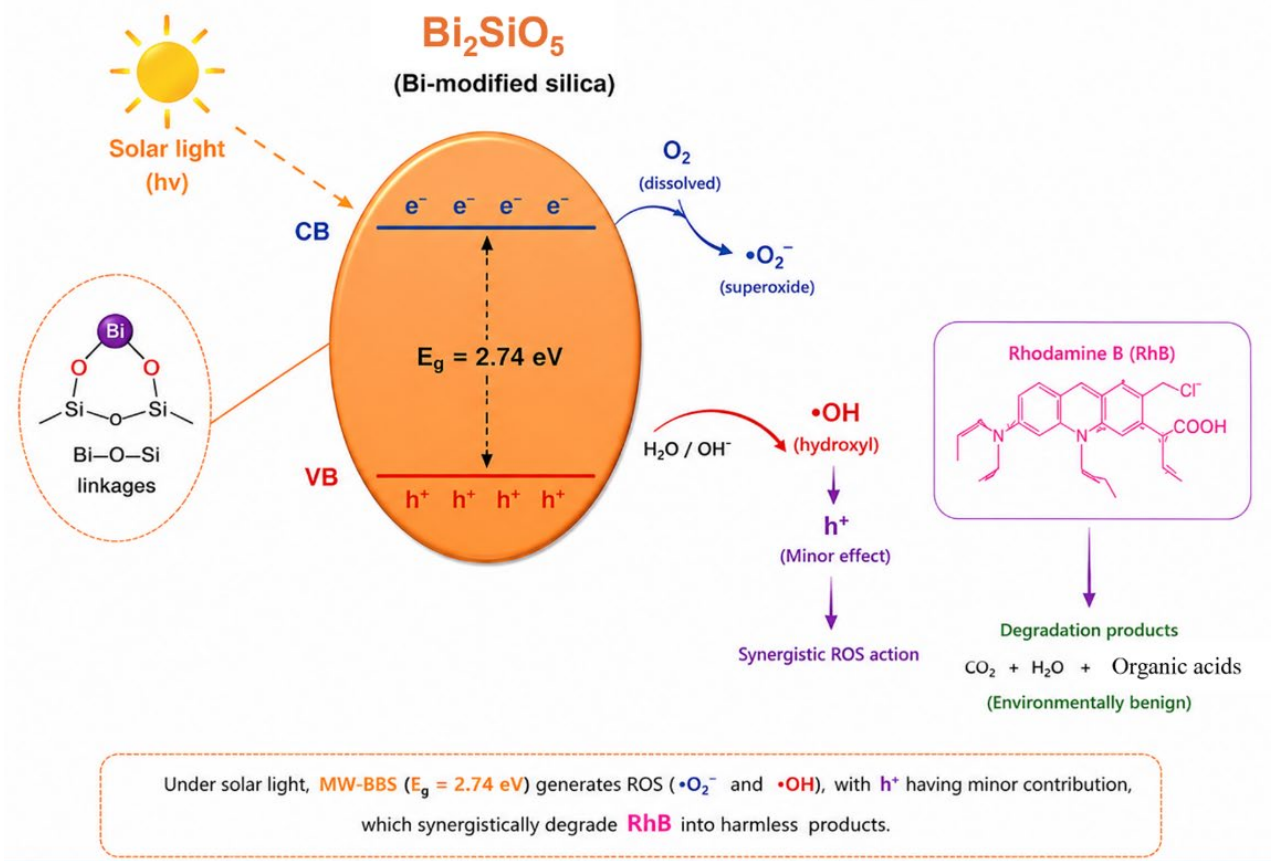

Figure 8. Proposed solar-driven photocatalytic mechanism and reactive oxygen species (ROS) pathways for the degradation of RhB over sand-derived Bi_2SiO_5 composites.

reaction time. Regarding the degradation of RhB, ultra-fast kinetics were observed, with Bi_2SiO_5 achieving total decolorization (99%) within 15 min (k_1 = 0.142 min^{-1}). When evaluated under higher initial dye concentrations, this performance remains highly competitive against reported systems. For instance, Bi_2S_3/Bi_2SiO_5 heterojunctions synthesized by Liu *et al.* which required 180 minutes to reach 87% degradation [4], and the Bi_2SiO_5 hierarchical microspheres reported by Dou *et al.* which required 80 min to reach 95% removal [14]. Furthermore, while Shafafi *et al.* synthesized binary TiO_2/Bi_2SiO_5 nanocomposites that required 180 min to reach 99.8% RhB degradation (10^{-5} M) under visible light [7], our sand-derived Bi_2SiO_5 achieved an equivalent removal level (99% at 10^{-5} M) in 15 min without requiring secondary semiconductor coupling (TiO_2) or complex multistep synthesis. Furthermore, our results are competitive with $Bi_2SiO_5/Bi_{12}SiO_{20}$ heterojunctions produced via microwave hydrothermal synthesis, which reached 97.5% removal in 30 min [29]. Although the Bi/Bi_2WO_6 (SPR) system reported by Chang *et al.* exhibited an identical reaction timeframe (15 min, 100% efficiency at 10 mg/L) [28], a comprehensive comparison reveals key operational trade-offs. The Bi/Bi_2WO_6 catalyst required a 12 h hydrothermal synthesis using synthetic Na_2WO_4 precursors, whereas our system utilizes natural sand as a sustainable, low-cost silica matrix prepared via a rapid 15 min microwave treatment. Therefore, while the intrinsic degradation rates under varying illumination conditions are comparable, the true advantage of the natural-sand-derived Bi_2SiO_5 lies in its balance between rapid catalytic activity, low synthesis energy demand, and green precursor utilization.

As highlighted in Table 2, direct quantitative benchmarking across literature studies remains complex due to unstandardized testing conditions (such as light intensity, reactor geometries, and catalyst-to-pollutant mass ratios). Nevertheless, when factoring in reaction rate, low operational dosage, and green precursor valorization, the present Bi_2SiO_5 nanocomposite demonstrates a highly efficient and sustainable alternative for solar-driven wastewater treatment.

4. Conclusion

This study successfully fulfills its core objective by establishing a rapid, energy-efficient, and sustainable paradigm for fabricating high-performance bismuth silicate (Bi_2SiO_5) photocatalysts directly from abundant natural sand, replacing costly commercial silicate precursors and multi-hour hydrothermal treatments with a fully microwave-driven co-precipitation and thermal processing route. The results confirm that unrefined mineral silica can direct the rapid nucleation of a predominantly phase-pure orthorhombic Bi_2SiO_5 structure alongside a minor secondary Bi_2O_3 phase, yielding a heterogeneous architecture that narrows the electronic bandgap into the visible regime and promotes strong dark adsorption together with efficient charge carrier separation under solar irradiation. Mechanistically, the dominant generation of hydroxyl and superoxide radical species drives stable and efficient solar photocatalytic degradation with robust cyclic reusability, while chemical oxygen demand evaluation confirms substantial (75%) partial mineralization of the target pollutant, going beyond simple adsorption or decolorization. These findings demonstrate that natural, low-cost mineral resources can be valorized into scalable catalytic media for solar-driven wastewater remediation. Future research will focus on full-profile Rietveld XRD refinement for quantitative phase modeling, LC-MS intermediate identification, continuous-flow photoreactor scale-up for real industrial effluents, and photo-electrochemical characterization (EIS, PL, and transient photocurrent) to fully map interfacial charge transport dynamics.

Table 2. Comparative evaluation of RhB removal performance with recent literature.

Photocatalyst	Si Precursor	Synthesis Method	Pollutant (Conc.)	Time (min)	RE (%)	Ref.
Bi_2S_3/Bi_2SiO_5	Na_2SiO_3	Ion Exchange (24 h)	RhB (20 mg/L)	180	87	[4]
$Bi_2Si_5/Bi_{12}SiO_{20}$	Nano-SiO_2	Microwave Hydrothermal	RhB (10 mg/L)	30	97.5	[5]
TiO_2/Bi_2SiO_5 (5%)	Na_2SiO_3	Hydrothermal (150 °C, 24 h)	RhB (1×10^{-5} M)	180	99.8	[7]
Bi_2SiO_5 (Spheres)	Na_2SiO_3	Solvothermal (24 h)	RhB (5 ppm)	80	95	[14]
Bi/Bi_2WO_6 (SPR)	Na_2WO_4	Hydrothermal (12 h)	RhB (10 mg/L)	15	100	[28]
Bi_2SiO_5	Natural Sand	Microwave (15 min)	RhB (1×10^{-5} M)	15	99	This work

Acknowledgment

The authors thank CINBIO (Universidade de Vigo) for providing access to the characterization facilities used in this work, and the University of Gabes for its financial support of the internship.

CRedit Author Statement

Author Contributions: Khouloud Benmarzoug: Writing, Methodology, Investigation, Software, Calculation, Data analysis, Interpretation and original draft. Chrifa Guerfel: Review & editing, Software. Mariem Ahbil: Review & editing, Software. Hédi Ben Amor: Review & editing, Conceptualization, Supervision, Validation. Noureddine Hamdi: Review & editing. All authors have read and agreed to the published version of the manuscript.

References

[1] Chen, C.C., Yang, C.T., Chung, W.H., Chang, J.L., Lin, W.Y. (2017). Synthesis and characterization of Bi4Si3O12, Bi2SiO5, and Bi12SiO20 by controlled hydrothermal method and their photocatalytic activity. *Journal of the Taiwan Institute of Chemical Engineers*, 78, 157–167. DOI: 10.1016/j.jtice.2017.05.021

[2] Patil, S.P., Bethi, B., Sonawane, G.H., Shrivastava, V.S., Sonawane, S. (2016). Efficient adsorption and photocatalytic degradation of Rhodamine B dye over Bi2O3-bentonite nanocomposites: A kinetic study. *Journal of Industrial and Engineering Chemistry*, 34, 356–363. DOI: 10.1016/j.jiec.2015.12.002

[3] Wu, Y., Hu, J., Wang, J., Han, L., Liu, Q., Xu, S. (2023). 3D cross-linked lamellar bismuth silicate with lamellar porous and double heterostructure and its photocatalytic performance under visible light. *Ceramics International*, 49(17), 28208–28215. DOI: 10.1016/j.ceramint.2023.06.075

[4] Liu, X., Pan, L., Lv, Y., Lu, Q., Lu, C., Xu, M., Zhu, Z. (2015). In situ synthesis of Bi2S3/Bi2SiO5 heterojunction photocatalysts with enhanced visible light photocatalytic activity. *RSC Advances*, 5(69), 55957–55963. DOI: 10.1039/c5ra09070a

[5] Zhang, Q., Liu, X., Liu, Y., Zhang, X., Yang, Y., Wang, Z. (2022). Microwave hydrothermal synthesis of a Bi2SiO5/Bi12SiO20 heterojunction with oxygen vacancies and multiple charge transfer for enhanced photocatalytic activity. *Applied Surface Science*, 581, 152337. DOI: 10.1016/j.apsusc.2021.152337

[6] Zhang, L., Wang, W., Sun, S., Jiang, D., Gao, E. (2013). Solar light photocatalysis using Bi2O3/Bi2SiO5 nanoheterostructures formed in mesoporous SiO2 microspheres. *CrystEngComm*, 15(46), 10043–10048. DOI: 10.1039/c3ce41433g

[7] Shafafi, S., Habibi-Yangjeh, A., Feizpoor, S., Chand, H., Krishnan, V., Wang, C. (2021). Impressive visible-light photocatalytic performance of TiO2 by integration with Bi2SiO5 nanoparticles: Binary TiO2/Bi2SiO5 photocatalysts with n-n heterojunction. *Colloids and Surfaces A: Physicochemical and Engineering Aspects*, 629, 127392. DOI: 10.1016/j.colsurfa.2021.127392

[8] Arefieva, O.D., Panasyuk, A.V., Novikov, A.A., Zemnukhova, L.A., Panov, A.M. (2023). Effect of silica source on photocatalytic properties of Bi2O3/Bi2SiO5 heterostructure. *Journal of Bioresources and Bioproducts*, 8(2), 176–186. DOI: 10.1016/j.jobab.2023.03.003

[9] Karthik, K., Devi, K.R.S., Pinheiro, D., Sugunan, S. (2019). Photocatalytic activity of bismuth silicate heterostructures synthesized via surfactant mediated sol-gel method. *Materials Science in Semiconductor Processing*, 102, 104589. DOI: 10.1016/j.mssp.2019.104589

[10] de Greñu, B.D., de los Reyes, R., Costero, A.M., Amorós, P., Ros-Lis, J.V. (2020). Recent progress of microwave-assisted synthesis of silica materials. *Nanomaterials*, 10(6), 1092. DOI: 10.3390/nano10061092

[11] Quang, H.T., Le Pham, H.A., Van Cuong, N., Dang, H.P., Anh, N.T.H. (2024). Rapid synthesis of Bismuth MOF @Carbon Nanotube Composite by microwave-assisted solvothermal for photodegrading RhB. *Topics in Catalysis*, 67(17–18), 1155–1168. DOI: 10.1007/s11244-024-01985-x

[12] Jan, S., Sharma, A., Srivastava, A., Dao, V.D., Sanghi, R. (2025). Enhanced photocatalytic ciprofloxacin degradation in industrial aquatic waste using CdS/Cs3Bi2Br9 nanocomposite synthesized by microwave energy. *Journal of Molecular Liquids*, 427, 127450. DOI: 10.1016/j.molliq.2025.127450

[13] Vasiljević, B.R., Stojadinović, S., Tadić, N., Radić, N., Grbić, B., Ćirić-Marjanović, G. (2026). Practical synthesis of nanostructured bismuth vanadate via fast and effective microwave-assisted method: Improved photocatalytic and electrochemical properties. *Surfaces and Interfaces*, 89, 109131. DOI: 10.1016/j.surfin.2026.109131

[14] Dou, L., Zhong, J., Li, J., Luo, J., Zeng, Y. (2019). Fabrication of Bi2SiO5 hierarchical microspheres with an efficient photocatalytic performance for rhodamine B and phenol removal. *Materials Research Bulletin*, 116, 50–58. DOI: 10.1016/j.materresbull.2019.03.031

[15] Le Jia, K., Qu, J., Hao, S. M., An, F., Jing, Y.Q., Yu, Z.Z. (2017). One-pot synthesis of bismuth silicate heterostructures with tunable morphology and excellent visible light photodegradation performances. *Journal of Colloid and Interface Science*, 506, 255–262. DOI: 10.1016/j.jcis.2017.07.040

[16] Joni, I.M., Nulhakim, L., Vanitha, M., Panatarani, C. (2018). Characteristics of crystalline silica (SiO2) particles prepared by simple solution method using sodium silicate (Na2SiO3) precursor. *Journal of Physics: Conference Series*, 1080, 012006. DOI: 10.1088/1742-6596/1080/1/012006

[17] Tsaviv, J.N., Eneji, I.S., Shato'Ato, R., Ahemen, I., Jubu, P.R., Yusof, Y. (2024). Photodegradation, kinetics and non-linear error functions of methylene blue dye using SrZrO3 perovskite photocatalyst. *Heliyon*, 10(14), e34517. DOI: 10.1016/j.heliyon.2024.e34517

[18] Tran, H.D., Nguyen, D.Q., Do, P.T., Tran, U.N.P. (2023). Kinetics of photocatalytic degradation of organic compounds: A mini-review and new approach. *RSC Advances*, 13(25), 17000–17015. DOI: 10.1039/d3ra01970e

[19] Police, A.K.R., Basavaraju, S., Valluri, D.K., Machiraju, S. (2013). Bismuth modified porous silica preparation, characterization and photocatalytic activity evaluation for degradation of isoproturon. *Journal of Materials Science & Technology*, 29(7), 639–646. DOI: 10.1016/j.jmst.2013.04.004

[20] Stepanova, A., Krivtsov, I., Ilkaeva, M., Garcia-Lopez, E.I., Marcì, G., Palmisano, L. (2023). TiO2 phase ratio's contribution to the photocatalytic activity. *ACS Omega*, 8(44), 41664–41673. DOI: 10.1021/acsomega.3c05890

[21] Joni, I.M., Vanitha, M., Panatarani, C., Faizal, F. (2020). Dispersion of amorphous silica nanoparticles via beads milling process and their particle size analysis, hydrophobicity and anti-bacterial activity. *Advanced Powder Technology*, 31(1), 370–380. DOI: 10.1016/j.apt.2019.10.029

[22] Pham, T.D., Hoang, T.C., Le, T.S., Nguyen, M.T., Le, H.A. (2021). Adsorptive removal of anionic azo dye new coccine using silica and silica-gel with surface modification by polycation. *Polymers*, 13(10), 1536. DOI: 10.3390/polym13101536

[23] Jiang, S., Zheng, G., Zhang, F., Yu, H., Cai, Y., Zhang, Y. (2026). CTAB-regulated Bi/Bi2WO6 heterojunction with effectively enhanced visible light photocatalytic degradation of pollutants. *Journal of Materials Science: Materials in Electronics*, 37(14), 1094. DOI: 10.1007/s10854-026-17487-3

[24] Chang, F., Lei, Y., Li, J., Li, S., Liu, D.G., Kong, Y. (2023). Externally modified Bi12SiO20 with BiOI: n-p heterojunctions for effectually photocatalytic degradation of bisphenol A. *Separation and Purification Technology*, 323, 124516. DOI: 10.1016/j.seppur.2023.124516

[25] Belik, Y.A., Vodyankin, A.A., Fakhrutdinova, E.D., Svetlichnyi, V.A., Vodyankina, O.V. (2022). Photoactive bismuth silicate catalysts: Role of preparation method. *Journal of Photochemistry and Photobiology A: Chemistry*, 425, 113670. DOI: 10.1016/j.jphotochem.2021.113670

[26] Dai, Z., Zhen, Y., Sun, Y., Li, L., Ding, D. (2021). ZnFe2O4/g-C3N4 S-scheme photocatalyst with enhanced adsorption and photocatalytic activity for uranium(VI) removal. *Chemical Engineering Journal*, 415, 129002. DOI: 10.1016/j.cej.2021.129002

[27] Zhu, F., Ma, J., Ji, Q., Cheng, H., Komarneni, S. (2021). Visible-light-driven activation of sodium persulfate for accelerating orange II degradation using ZnMn2O4 photocatalyst. *Chemosphere*, 278, 130404. DOI: 10.1016/j.chemosphere.2021.130404

[28] Rajan, G., Rajput, R.B., Shaikh, R.S., Kale, R.B. (2025). Hydrothermally engineered highly active Bi2WO6 photocatalyst for the degradation of Rhodamine B, Bisphenol A and dye mixture under visible light irradiation. *Inorganic Chemistry Communications*, 177, 114430. DOI: 10.1016/j.inoche.2025.114430.